

## Role of friction stir welding parameters on tensile strength of AA6061–B<sub>4</sub>C composite joints

K. KALAISELVAN<sup>1</sup>, N. MURUGAN<sup>2</sup>

1. Department of Mechatronics Engineering, Kongu Engineering College,  
Perundurai, Erode–638052, Tamil Nadu, India;

2. Department of Mechanical Engineering, CIT, Coimbatore–641 014, Tamil Nadu, India

Received 29 January 2012; accepted 18 April 2012

**Abstract:** Friction stir welding (FSW) is a solid state joining technique developed to join high strength aluminum alloys and various ceramic reinforced metal matrix composites (MMCs). FSW produces sound welds in MMCs without any deleterious reaction between reinforcement and matrix. The present work focused on the effect of FSW parameters on the tensile strength of Al–B<sub>4</sub>C composite joints. The central composite design of four factors and five levels was used to control the number of experiments. A mathematical model was developed to analyze the influence of FSW parameters. The results indicated that the joint fabricated using rotational speed of 1000 r/min, welding speed of 1.3 mm/s, axial force of 10 kN and the reinforcement of 12% showed larger tensile strength compared with the other joints. The developed model was optimized to maximize the tensile strength using generalized reduced gradient method. The metallographic analysis of the joints showed the presence of various zones such as weld nugget (WN) zone, thermo mechanically affected zone (TMAZ) and heat affected zone (HAZ). The substantial grain refinement of aluminum matrix as well as significant size reduction of B<sub>4</sub>C particles was observed in the weld nugget. TMAZ was plastically deformed, thermally affected and exhibited elongated aluminum grains.

**Key words:** friction stir welding; metal matrix composites; boron carbide; joint; mechanical properties

### 1 Introduction

Boron carbide reinforced aluminum matrix composites (AMCs) are more focused in nuclear industries because of their good chemical and thermal stability. The aluminum based boron and metallic composites are currently used as neutron absorber material in nuclear power plants [1,2]. In addition, AMCs absolutely possess good mechanical and physical properties such as light weight, high strength, high specific modulus, low coefficient of thermal expansion and good wear resistant. But joining of composites by fusion welding process brings certain limitation on the mechanical properties. During the fusion welding, the Al matrix undergoes problems like high thermal expansion and conductivity, high solubility of gases in molten metal, solidification shrinkages and deleterious reactions with reinforcement [3,4]. Hence, a solid state welding is preferred for joining AMCs to produce a sound weld.

Friction stir welding is a relatively new solid state joining process invented by The Welding Institute (TWI) in Cambridge, UK in 1991. During the welding, a special shaped FSW tool is rotated, plunged and then traversed along the joint to form weld. Now, FSW has been used to weld the monolithic materials such as aluminum, magnesium, steel. Recently, several studies have reported that the FSW produces a high quality weld joint in aluminum based composites [5,6]. FSW process eliminates all the fusion welding problems as mentioned earlier. However, the presence of hard ceramic reinforcement particles in the composites offers high wear resistance which affects the weld quality [5]. The material flow behavior of MMCs during FSW process greatly depends on the welding parameters, tool design and the amount of reinforcement. The weld temperature and rotation of tool also influence the particle size, shape and distribution in the weld zone [7,8]. It has been reported that the square pin profile produces a better tensile strength when joining MMCs than the other

profiles [9]. CHEN et al [7] reported that the joint efficiency of friction stir welded AA6063–B<sub>4</sub>C is higher than 60% and increased to 80% after aging. Hence, an attempt has been made to develop a mathematical model to predict the tensile strength of friction stir welded AA6061–B<sub>4</sub>C composite incorporating welding parameters such as rotational speed ( $N$ ), welding speed ( $S$ ), and axial load ( $F$ ), and reinforcement ( $R$ ) using design of experiments. The effects of various parameters on tensile strength, joint efficiency and the microstructure are examined.

## 2 Experimental

The B<sub>4</sub>C reinforced aluminum matrix composites were fabricated by modified stir casting route. The chemical composition of Al matrix is shown in Table 1. The B<sub>4</sub>C having a size of 10  $\mu\text{m}$  was added along with equal quantity of K<sub>2</sub>TiF<sub>6</sub> flux into the aluminum molten metal to obtain AMCs. AMCs having different mass fraction of B<sub>4</sub>C were produced. The details of fabrication are available in Ref. [10]. The mechanical properties of the produced composites are presented in Table 2. The plates with dimensions of 100 mm×50 mm×6 mm were obtained from the fabricated AMCs by slicing them using a power hacksaw machine. A special purpose friction stir welding machine was used to conduct the experiment. A high carbon high chromium (HCHCr) steel tool oil hardened to HRC 62 having square pin profile was fabricated and the details of the fabricated FSW tool are shown in Fig. 1.

The process parameters such as rotational speed ( $N$ ), welding speed ( $S$ ), axial load ( $F$ ) and reinforcement ( $R$ ) were considered in the present study [7,11]. Initial trial

**Table 1** Chemical composition of aluminum alloy (6061-T6) (mass fraction, %)

Mg	Si	Fe	Cu	Mn
0.95	0.54	0.22	0.17	0.13
Cr	Zn	Ti	Al	
0.09	0.08	0.01	Bal.	

**Table 2** Mechanical properties of produced Al–B<sub>4</sub>C composites

No.	B <sub>4</sub> C mass fraction in Al matrix/%	Ultimate tensile strength/MPa	Micro hardness (VHN)	Macro hardness (BHN)
1	0	160	45	30
2	4	185	51.3	34.4
3	6	191	58.5	38.9
4	8	199	69.6	43.6
5	10	206	75.5	50.3
6	12	215	80.8	58.6

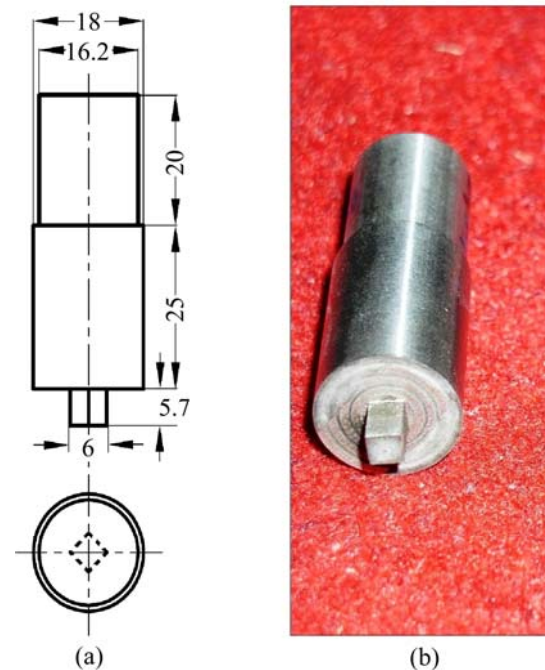


**Fig. 1** FSW Tool: (a) Dimensions; (b) Fabricated tool (Unit: mm)

runs were carried out to obtain the working range of those process parameters to produce a defect-free joint. The selected ranges of process parameters and their levels are shown in Table 3. The upper limit of a parameter was coded as +2 and its lower limit was coded as -2. The intermediate coded values can be calculated from the relationship [12]:

$$X_i = 2[2X - (X_{\max} + X_{\min})] / (X_{\max} - X_{\min}) \quad (1)$$

where  $X_i$  is the required coded value of a variable  $X$ ;  $X$  is the any value of the variable from  $X_{\min}$  to  $X_{\max}$ ;  $X_{\min}$  is the lower level of the variable;  $X_{\max}$  is the upper level of the variable.

**Table 3** FSW process parameters ranges and levels

Process parameter	Notation	Level				
		-2	-1	0	1	2
Rotational speed/(r·min <sup>-1</sup> )	$N$	800	900	1000	1100	1200
Welding speed/(mm·s <sup>-1</sup> )	$S$	0.3	0.8	1.3	1.8	2.3
Axial force/kN	$F$	6	8	10	12	14
Reinforcement/%	$R$	4	6	8	10	12

A four-factor and five-level central composite design having 31 runs was used to conduct the experiments [8, 12–14]. The developed design matrix is shown in Table 4. As per the design matrix, 31 butt joints

were fabricated using the FSW machine. Three tensile specimens were prepared from each of the welded plates obtained by cross sectioning at the centre perpendicular to the welding direction according to ASTM E08 standard [15]. The dimension of tensile specimen is presented in Fig. 2. The ultimate tensile strength (UTS) was evaluated using a computerized universal tensile testing machine (TUE-C-1000). The joint efficiency was estimated by calculating the ratio of UTS of friction stir welded joint to UTS of base metal. The average UTS and joint efficiency for all 31 joints are presented in Table 4.

**Table 4** Design matrix with experimental results

Trial run	Design matrix				Estimated UTS/MPa	Joint efficiency/%
	<i>N</i>	<i>S</i>	<i>F</i>	<i>R</i>		
1	-1	-1	-1	-1	146.2	76.54
2	+1	-1	-1	-1	137.1	71.78
3	-1	+1	-1	-1	131.5	68.85
4	+1	+1	-1	-1	139.3	72.93
5	-1	-1	+1	-1	148.8	77.91
6	+1	-1	+1	-1	142.2	74.45
7	-1	+1	+1	-1	150.5	78.80
8	+1	+1	+1	-1	141.3	73.98
9	-1	-1	-1	+1	163.9	79.56
10	+1	-1	-1	+1	154.2	74.85
11	-1	+1	-1	+1	165.7	80.44
12	+1	+1	-1	+1	159.3	77.33
13	-1	-1	+1	+1	142.9	69.37
14	+1	-1	+1	+1	151.4	73.50
15	-1	+1	+1	+1	158.2	76.80
16	+1	+1	+1	+1	149.3	72.48
17	-2	0	0	0	124.7	62.66
18	+2	0	0	0	131.5	66.08
19	0	-2	0	0	121.1	60.85
20	0	+2	0	0	136.2	68.44
21	0	0	-2	0	128.8	64.72
22	0	0	+2	0	138.3	69.50
23	0	0	0	-2	175.5	94.86
24	0	0	0	+2	200.1	93.06
25	0	0	0	0	188.5	94.72
26	0	0	0	0	181.7	91.31
27	0	0	0	0	179.8	90.35
28	0	0	0	0	185.4	93.17
29	0	0	0	0	183.2	92.06
30	0	0	0	0	186.5	93.72
31	0	0	0	0	185.1	93.02

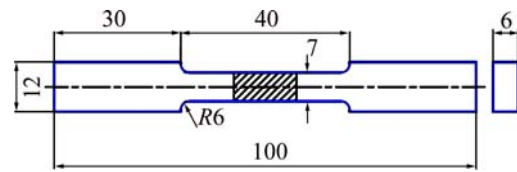


**Fig. 2** Dimensions of tensile specimen (ASTM E08) (unit: mm)

The metallographic samples were obtained as per standard metallographic procedure from the transverse section of the welded plate. The macro etching was done using 5% NaOH solution. The macrostructures were captured using a digital optical scanner and presented in Table 5. The specimen from trail run No. 24 in Table 4 was used for microstructure analysis and colour etched with a reagent having 4 g of potassium permanganate, 1 g of sodium hydroxide dissolved in 100 mL distilled water. The microstructure was observed using an optical metallurgical microscope (Olympus Microscope–BX51M) and a scanning electron microscope (JEOL JSM–6390). The observed optical and SEM micrographs of different zones and fracture morphology are shown in Figs. 3, 4 and 5, respectively.

### 3 Development of mathematical model

The response function representing the tensile strength ( $\sigma$ ) of friction stir welded Al–B<sub>4</sub>C joints can be expressed as follows:

$$\sigma = f(N, S, F, R) \quad (2)$$

The second order polynomial (regression) equation used to represent the response surface ( $Y$ ) can be expressed as

$$Y = b_0 + \sum b_i X_i + \sum b_{ii} X_i^2 + \sum b_{ij} X_i X_j \quad (3)$$

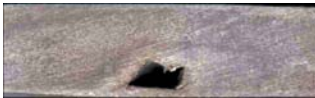
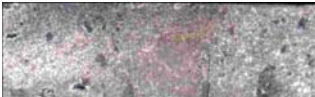
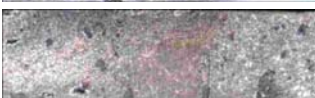
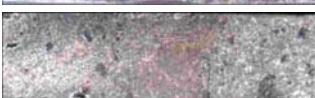
For four factors, the selected polynomial could be expressed as

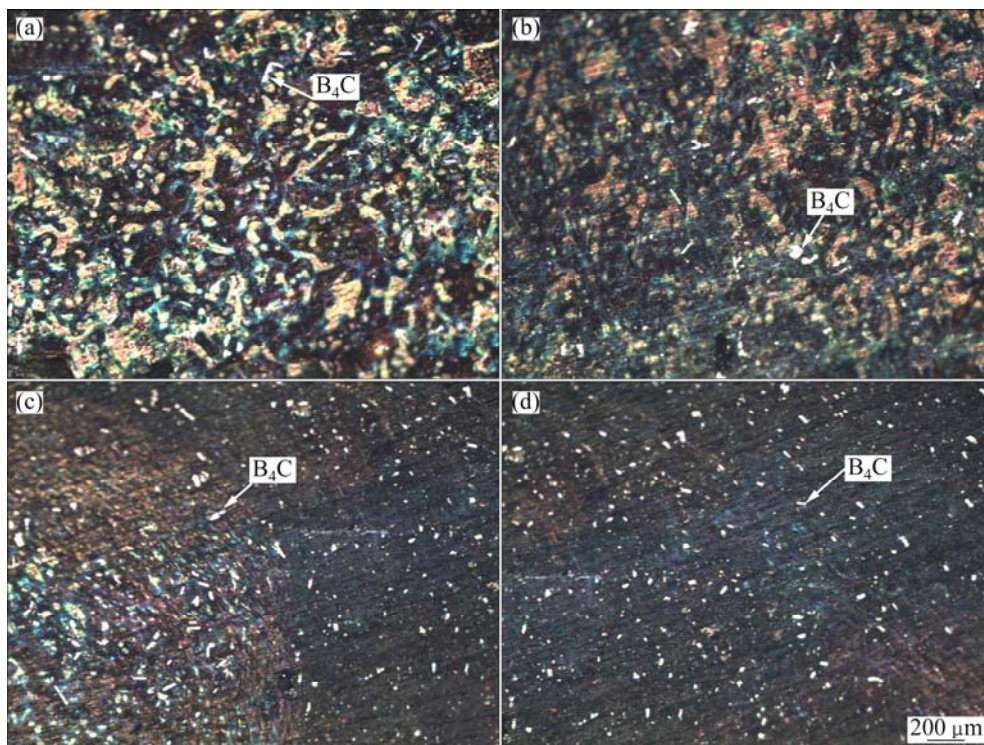
$$\sigma = b_0 + b_1 N + b_2 S + b_3 F + b_4 R + b_{11} N^2 + b_{22} S^2 + b_{33} F^2 + b_{44} R^2 + b_{12} NS + b_{13} NF + b_{14} NR + b_{23} SF + b_{24} SR + b_{34} FR \quad (4)$$

where  $b_0$  is the average of responses and  $b_1, b_2, \dots, b_{34}$  are the response coefficients that depend on the main and interaction effects of the parameters. All the coefficients were evaluated and the initial model was developed using a statistical software package (SYSTAT 12). After determining the significant coefficients, the final model was developed by eliminating least and insignificant terms. The developed mathematical model for predicting the tensile strength of FSW joints is given below.

$$\sigma = 186.262 - 0.833N + 1.608S + 0.267F + 6.800R - 13.596N^2 - 13.459S^2 - 12.234F^2 - 4.375FR \quad (5)$$

**Table 5** Effect of FSW parameters on macrostructure of Al/B<sub>4</sub>C composite

Trial run	Process parameter	Macrostructure	Defect	Probable reason
17	Rotational speed/ (r·min <sup>-1</sup> )	800 	Tunnel defect	Poor plasticized of metal due to low heat generation
25		1000 	No defect	Adequate stirring and heat input
18		1200 	Tunnel defect	Excessive stirring and flash of plasticized material
19	Welding speed/ (mm·s <sup>-1</sup> )	0.3 	Pin hole	Poor consolidation of material
25		1.3 	No defect	Adequate heat generation and transportation of material
20		2.3 	Tunnel defect	In Adequate heat input and low frictional heat generation
21	Axial force/ kN	6 	Tunnel defect	Insufficient axial force and heat generation
25		10 	No defect	Sufficient flow of plasticized material
22		14 	Worm hole	High frictional heat generation

**Fig. 3** Optical micrographs of transverse section of cast AA6061–B<sub>4</sub>C MMCs (trail run No. 24): (a) Base metal (BM); (b) Heat affected zone (HAZ); (c) Thermomechanically affected zone (TMAZ); (d) Weld nugget (WN)

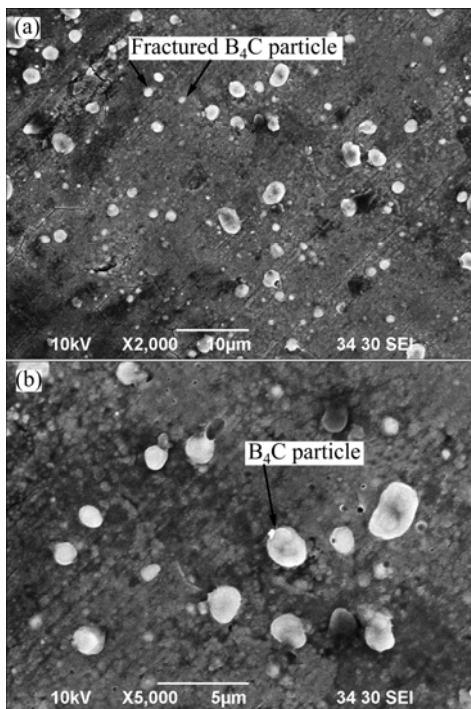


**Fig. 4** SEM micrographs of transverse section of cast AA6061–B<sub>4</sub>C MMCs (trail run No. 24)

#### 4 Adequacy of developed model

The adequacy of the developed model was tested by analysis of variance (ANOVA) with the help of SYSTAT software and the results are shown in Tables 6 and 7. In this case, the value of  $R^2$  is 0.951 and the adjusted  $R^2$  is 0.933. If the value of  $R^2$  is 1.0, the predicted model values exactly coincide with the experimental values. A higher value of  $R^2$  indicates that the regression model is quite adequate [16]. Table 7 shows the calculated value of  $F$  ratio which is greater than the tabulated value at 95% of confidential level, indicating the adequacy of the model.

#### 5 Conformity test

Five confirmation experiments were conducted with different values of process parameters other than those mentioned in the design matrix to verify the developed regression model. The UTS of the welded plates was estimated and compared with the corresponding predicted UTS using Eq. (5), as presented in Table 8. From the table the average error is found to be 1.27%, which indicates that the model is accurate.

**Table 7** Analysis of variance (ANOVA) for developed model

Response	Source	Sum of square	Degree of freedom	Mean square	Calculated $F$ -ratio	Tabulated $F$ -ratio
UTS	Regression	14013.649	8	1751.706	53.084	2.40
	Residual	725.968	22	32.999		

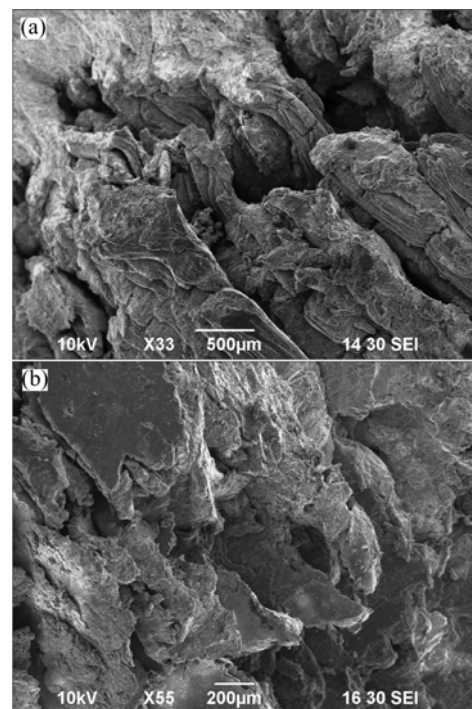


**Fig. 5** Fractographs of friction stir welded tensile test specimen (trail run No. 24)

#### 6 FSW parameters optimization

The FSW parameters significantly influence the UTS of welded joints. It is necessary to select the right combination of parameters to maximize tensile strength. The regression equation obtained from the developed model was used to optimize the FSW parameters using generalized reduced gradient method (GRG). The optimization is a nonlinear constrained maximization problem and is solved using GRG which is embedded in MS Excel solver module. The following constraints were considered for optimizing the UTS from Eq. (5).

$$\begin{aligned} -2 &\geq N \leq +2 \\ -2 &\geq S \leq +2 \\ -2 &\geq F \leq +2 \\ -2 &\geq R \leq +2 \end{aligned}$$

The optimized welding parameters are: rotational

**Table 6** Statistical result for developed model

Response	Multiple $R$	Squared multiple $R$	Adjusted squared multiple $R$	Standard error of estimation
UTS	0.975	0.951	0.933	5.744

**Table 8** Conformity of test result

No.	FSW process parameter				UTS		
	<i>N</i>	<i>S</i>	<i>F</i>	<i>R</i>	Experimental value/MPa	Predicted value/MPa	Error/%
1	1.25	-1.5	-1.25	-2	95.01	87.30	8.84
2	0.75	-0.25	0.5	-1	159.81	169.21	-5.55
3	0.25	-0.75	1.5	0	144.87	149.30	-2.97
4	-0.5	0.75	0.75	1	187.65	173.75	8.00
5	-1.5	-1.25	-0.5	2	145.78	148.66	-1.94
Average							1.27

speed of 997 r/min; welding speed of 1.3 mm/s; axial force of 9.3 kN; reinforcement of 12%; and the predicted optimized tensile strength is 201.4 MPa. The FSW was carried out for the optimized parameter on the composite plates and the estimated UTS value is 208.2 MPa. The error is 3.4%.

## 7 Results and discussion

The developed mathematical model was used to evaluate the influence of process parameters on UTS of friction stir welded Al-B<sub>4</sub>C composite joints.

### 7.1 Microstructure analysis

The microstructural behavior of friction stir welded Al-B<sub>4</sub>C composite joint was studied. The micrographs shown in Figs. 3(a)–(d) correspond to BM, HAZ, TMAZ and WN respectively depicting the variations in grain size for the rotational speed of 1000 r/min, welding speed of 1.3 mm/s, axial force of 10 kN and reinforcement of 12%.

The micrograph of base metal as shown in Fig. 3(a) reveals the coarse grain structure with homogeneous dispersion of reinforcement of B<sub>4</sub>C particles in the matrix. After FSW, the substantial grain refinement of matrix and reduction in B<sub>4</sub>C particle size were observed in Fig. 3(d) in the stir zone. Elongated grains were observed (Fig. 3(c)) in the TMAZ. No significant change in microstructure was obtained in the HAZ (Fig. 3(b)) compared to BM.

During the FSW process, the stir zone is subjected to severe plastic deformation and material flow takes place due to stirring action of the tool pin. The frictional heat generated during the process is responsible for grain refinement. The stirring effect by the pin closed the casting porosity as well as abraded the surface of the B<sub>4</sub>C particles into small pieces. The fractured particles can be evident from SEM photomicrograph shown in Fig. 4(a). The well bonding of reinforcement in the matrix is observed from Fig. 4(b). The presence of such numerous small and round particles with fine grain matrix significantly improved the mechanical properties of the

weld joint.

Figure 5 shows the fracture surface of the tensile tested specimen. In general, the failure mechanisms of particulate reinforced composites are: 1) cracking the large reinforcing particles, 2) interfacial de-cohesion at the particle-matrix interface, resulting in nucleation of voids and 3) growth and coalescence of voids in the matrix [3]. The presence of flakes and micro voids in the fractographs shown in Fig. 5 might have promoted the brittle failure of the matrix. The local stress produced may not be sufficient to crack the reinforcement particles.

### 7.2 Effect of rotational speed on UTS

Figure 6 shows the effect of tool rotational speed on UTS of friction stir welded AA6061-B<sub>4</sub>C composite joint. The maximum tensile strength was obtained at the rotational speed of 1000 r/min. At a lower rotational speed (800 r/min) and higher rotational speed (1200 r/min), the tensile strength of joint was poor. When the rotational speed was increased from 800 r/min, correspondingly the UTS also increased and reached a maximum at 1000 r/min. If the rotational speed was increased above 1000 r/min, the UTS of the joint was decreased.

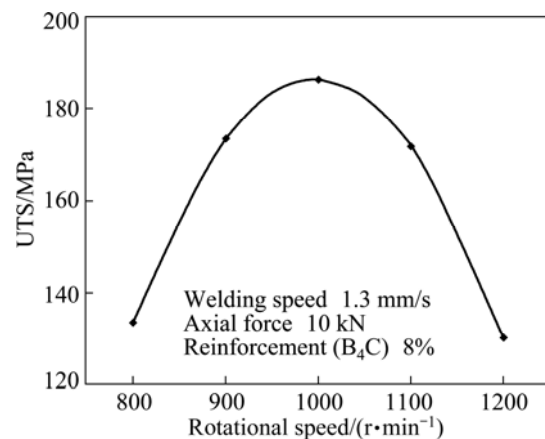


**Fig. 6** Effect of tool rotational speed on UTS of AA6061-B<sub>4</sub>C composite joint

A lower tool rotational speed (800 r/min) produced a lower heating condition as well as poor stirring action by the tool pin and improper consolidation of work material by the tool shoulder [17]. Hence a lower tensile strength was obtained. The increase in rotational speed increased the heat input per unit length of the joint, which causes a greater uniform grain refinement resulting in improved tensile strength. A very significant increase in the rotational speed (i.e. more than 1000 r/min) may produce an excessive release of stirred material on the top surfaces, which resulted in the formation of micro voids into the stirred zone. The rise in temperature as well as lower cooling rate and coarsening of grains at more than desired temperature may also reduce the tensile properties at high rotational speed. The macroscopic observation showed a tunnel defect in the weld zone at 800 r/min and 1200 r/min, as shown in Table 5. It may be attributed to discontinuities in the velocity field during the FSW process around the rotating tool. The typical defects occur when the material flows around the advancing side of the weld because there is no force promoting its movement back into the volume stirred by the moving tool [18].

### 7.3 Effect of welding speed on UTS

Figure 7 shows the effect of welding speed on UTS of friction stir welded AA6061–B<sub>4</sub>C composite joint. The UTS of FSW joint was low at the lower welding speed of 0.3 mm/s. The UTS value was increased with increase in welding speed until the maximum of 1.3 mm/s. Further increase in welding speed decreased the UTS of FSW joint.

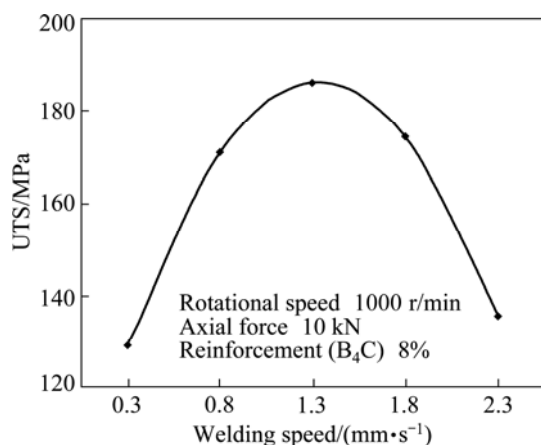


**Fig. 7** Effect of welding speed on UTS of AA6061–B<sub>4</sub>C composite joint

It can be observed that a higher welding speed decreases the frictional heat input to the work material, which creates poor plastic flow of the metal and causes some voids like defects in the welded joint. This restricts grain growth and causes reduction in the width of the

weld. Hence poor tensile strength is obtained. When the welding speed is slower than a certain critical value, it can produce a defect-free joint with improved UTS. The grain structures in the nugget zone were investigated to study the effect of welding speed on microstructure. The OM (Fig. 3(d)) and SEM (Fig. 4(a)) images show the equiaxed grain structure in the WN. The grain refinement with dispersion of B<sub>4</sub>C particle increases the tensile properties of the joint. The macrograph presented in Table 5 shows the presence of pin hole and tunnel defects both at lower welding speed of 0.3 mm/s and higher welding speed of 2.3 mm/s for the experimental work.

### 7.4 Effect of axial force on UTS

Figure 8 shows the effect of axial force on UTS of friction stir welded AA6061–B<sub>4</sub>C composite joints. The lowest strength was obtained at axial load of 6 kN and 14 kN. The UTS of composite joint was increased with increase in axial load up to a maximum load of 10 kN. Further increase in axial load decreased the tensile strength of the joint.

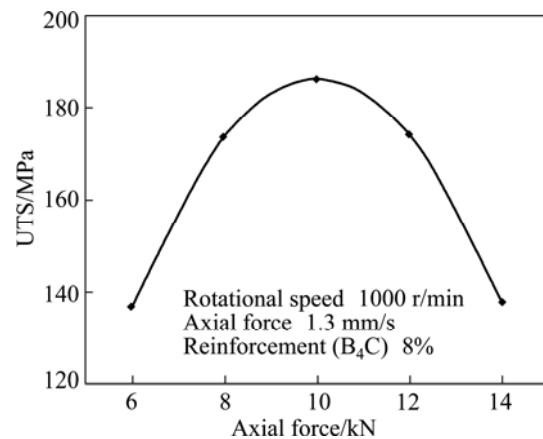


**Fig. 8** Effect of axial force on UTS of AA6061–B<sub>4</sub>C composite joint

During the FSW process, the rotation of tool produces a large amount of heat input which brings the metal to become very hot and plastic state. The axial force is more responsible for the plunge depth of the tool pin into the work piece [8]. The joining of materials depends on the extrusion process by axial force and the rotation of tool pin which propel the plasticized material. At a lower axial force (6 kN), the lowest frictional heat is generated which is not sufficient to generate a adequate plastic state. At a higher axial force (14 kN) the plunge depth of the tool into the work piece is higher which drastically decreases the strength [13]. Hence, lower or higher axial force resulted in inferior tensile strength. The joint fabricated with an axial force (10 kN) produced a finer grain structure with uniform distribution of

reinforcement particle in the stir zone and resulted higher UTS value. Hence sufficient axial force is required to form good weld. The macrostructure shown in Table 5 on experimental condition reveals the presence of tunnel and worm hole defect at 6 kN and 14 kN respectively.

### 7.5 Effect of B<sub>4</sub>C reinforcement on UTS

Figure 9 shows the effect of B<sub>4</sub>C reinforcement on the UTS of friction stir welded composite joint. The increase in the amount of reinforcement of B<sub>4</sub>C particle in the composite increased the tensile strength and reduced the ductility of composites. During the FSW process, the reinforcement particles were broken down and spread uniformly around the surface of rotating tool due to stirring effect which is observed in the SEM micrograph shown in Fig. 4(a). The extrusion process also reduced the size and concentration of particle clusters in the composite compared to the parent composite.

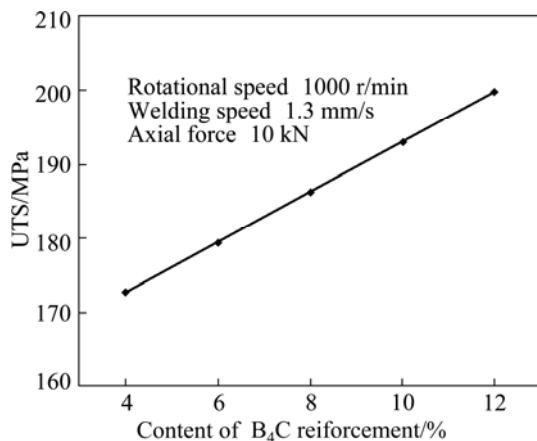


Fig. 9 Effect of B<sub>4</sub>C reinforcement on UTS of AA6061–B<sub>4</sub>C composite joint

### 7.6 Interaction effect of axial force and B<sub>4</sub>C reinforcement on UTS

The interaction effect of axial force and B<sub>4</sub>C reinforcement is shown in Fig. 10. In general, the degree of material mixing, interdiffusion, deformation of aluminum lamellae and material flow patterns highly depend on the welding temperature, flow stress and axial force [19]. From the figure it can be observed that the UTS of composite joint was increased with increase in axial force until the maximum of 10 kN for all levels of reinforcement. The higher UTS value of 199.86 kN and lower UTS value of 172.66 kN were obtained at 12% and 4% of B<sub>4</sub>C reinforcement respectively. Further increase in axial force decreased the UTS value and merged at a common point irrespective of reinforcement. It may be due to the formation of hydrostatic pressure and high heat input at higher axial force along the joint which affects the quality of weld. During the FSW

process the presence of reinforcement particles increases the nucleation sites and consequently, reduces the grain size of the matrix [3]. Hence the strength of composite joint is increased with the amount of reinforcement content.

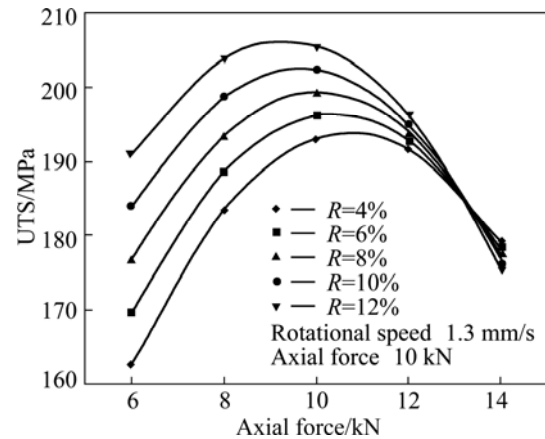


Fig. 10 Interaction effect of axial force and B<sub>4</sub>C reinforcement (R) on UTS of AA6061–B<sub>4</sub>C composite joint

## 8 Conclusions

- 1) Mathematical model was developed to predict the UTS of friction stir welded Al–B<sub>4</sub>C composite joint.
- 2) The process parameters significantly influence the tensile strength of weld joints.
- 3) The process parameters were optimized using GRG method.
- 4) Microstructure of welded Al–B<sub>4</sub>C composite exhibits fine and recrystallized grains of Al matrix with uniform distribution of B<sub>4</sub>C particle in the NZ.

## Acknowledgement

The authors gratefully thank the Management and Welding Research Cell, Department of Mechanical Engineering, Coimbatore Institute of Technology, Coimbatore, India for providing the welding equipment facilities to carry out this research work. The authors wish to express thanks to Naval Research Board, DRDO, Govt. of INDIA, vide funded project; Ref. no. DNRD/05/4003/NRB/85 dt 30.10.2006 for sponsoring FSW machine. The authors are grateful to Karunya University for providing SEM, UTM testing facilities and to Mr. S. J. VIJAY and Mr. I. DINAHARAN for their technical support offered to execute the research work.

## References

- [1] ABENOJAR J, VELASCO F, MARTINEZ M A. Optimization of processing parameters for the Al+10%B<sub>4</sub>C system obtained by mechanical alloying [J]. Journal of Materials Processing Technology,

- 2007, 184(1–3): 441–446.
- [2] SHOROWORDI K M, LAOUI T, HASEEB A S M A, CELIS J P, FROYEN L. Microstructure and interface characteristics of B<sub>4</sub>C, SiC, and Al<sub>2</sub>O<sub>3</sub> reinforced Al matrix composites: A comparative study [J]. *Journal of Materials Processing Technology*, 2003, 142(3): 738–743.
- [3] CESCHINI L, BOROMEI I, MINAK G, MORRI A, TARTERINI F. Effect of friction stir welding on microstructure, tensile and fatigue properties of the AA7005/10Vol.%Al<sub>2</sub>O<sub>3p</sub> composite [J]. *Composites Science and Technology*, 2007, 67(3–4): 605–615.
- [4] MARZOLI L M, STROMBECK A V, DOS SANTOS J F, GAMBARO C, VOLPONE L M. Friction stir welding of an AA6061/Al<sub>2</sub>O<sub>3</sub>20P reinforced alloy [J]. *Composites Science and Technology*, 2006, 66(2): 363–371.
- [5] FENG A H, XIAO B L, MA Z Y. Effect of microstructural evaluation on mechanical properties of friction stir welded AA2009/SiC<sub>p</sub> [J]. *Composites Science and Technology*, 2008, 68(9): 2141–2148.
- [6] UZUN H. Friction stir welding of SiC particulate reinforced AA2124 aluminum alloy matrix composite [J]. *Materials & Design*, 2007, 28(5): 1440–1446.
- [7] CHEN X G, SILVA M D, GOUGEON P, ST-GEORGES L. Microstructure and mechanical properties of friction stir welded AA6063–B<sub>4</sub>C metal matrix composites [J]. *Materials Science and Engineering A*, 2009, 518(1–2): 174–184.
- [8] ELANGO VAN K, BALASUBRAMANIAN V, BABU S. Predicting tensile strength of friction stir welded AA6061 aluminum alloy joints by a mathematical model [J]. *Materials & Design*, 2009, 30(1): 188–193.
- [9] VIJAY S J, MURUGAN N. Effect of tool pin profile on the metallurgical and tensile properties of friction stir welded Al-TiB<sub>2</sub> metal matrix composite [J]. *Materials & Design*, 2010, 31(7): 3585–3589.
- [10] KALAISELVAN K, MURUGAN N, PARAMESWARAN S. Production and characterization of AA6061–B<sub>4</sub>C stir cast composite [J]. *Materials & Design*, 2011, 32(7): 4004–4009.
- [11] GOPALAKRISHNAN S, MURUGAN N. Prediction of tensile strength of friction stir welded aluminium matrix TiCp particulate reinforced composite [J]. *Materials & Design*, 2011, 32(1): 462–467.
- [12] ELANGO VAN K, BALASUBRAMANIAN V, BABU S. Developing an empirical relationship to predict tensile strength of friction stir welded AA2219 aluminium alloy [J]. *Materials & Design*, 2008, 17(6): 820–830.
- [13] SUNDARAM S N, MURUGAN N. Tensile behavior of dissimilar friction stir welded joints of aluminium alloys [J]. *Materials & Design*, 2010, 31(9): 4184–4193.
- [14] MONTGOMERY D G. *Design and analysis of experiments* [M]. 5th ed. John Wiley & Sons, 2001.
- [15] Standard test method for tension testing of metallic materials, ASTM Standard E8 [R]. West CONSHOHOCHEN (USA): ASTM International, 2004.
- [16] PALANI P K, MURUGAN N. Development of mathematical models for prediction of weld bead geometry in cladding by flux cored arc welding [J]. *International Journal Advanced Manufacturing Technology*, 2006, 30(7–8): 669–676.
- [17] KARTHIKEYAN L, SENTHIL KUMAR V S, PADMANABHAN K A. On the role of process variables in the friction stir cast aluminum A319 alloy [J]. *Materials & Design*, 2010, 31(2): 761–771.
- [18] AZIMZADEGAN T, SERAJZADEH S. An investigation into microstructures and mechanical properties of AA7075-T6 during friction stir welding at relatively high rotational speeds [J]. *Journal of Materials Engineering Performance*, 2010, 19(9): 1256–1263.
- [19] ELANGO VAN K, BALASUBRAMANIAN V. Influences of tool pin profile and tool shoulder diameter on the formation of friction stir processing zone in AA6061 aluminum alloy [J]. *Materials & Design*, 2008, 29(2): 362–373.

## 搅拌摩擦焊接工艺参数对 AA6061–B<sub>4</sub>C 焊接接头抗拉强度的影响

K. KALAISELVAN<sup>1</sup>, N. MURUGAN<sup>2</sup>

1. Department of Mechatronics Engineering, Kongu Engineering College,  
Perundurai, Erode-638052, Tamil Nadu, India;

2. Department of Mechanical Engineering, CIT, Coimbatore–641 014, Tamil Nadu, India

**摘要:** 搅拌摩擦焊(FSW)是一种固态连接技术, 可用于连接高强度铝合金及多种陶瓷颗粒增强金属基复合材料(MMCs)。搅拌摩擦焊获得的陶瓷增强金属基复合材料焊缝优良, 在增强体与基体间没有发生有害反应。对搅拌摩擦焊接工艺参数对 AA6061–B<sub>4</sub>C 焊接接头抗拉强度的影响进行研究。采用 4 因素 5 水平的中心复合设计来控制实验的次数。构建一数学模型来分析搅拌摩擦焊接工艺参数对接头抗拉强度的影响。结果表明, 在旋转速度 1000 r/min、焊接速度 1.3 mm/s、轴向力 10 kN、增强相含量 12%的条件下, 搅拌摩擦焊得到的焊接接头的抗拉强度最大。根据构建的模型采用广义简约梯度算法进行优化以得到最大的抗拉强度。金相分析表明, 在焊接接头中出现了多种区域, 如焊合区、热力影响区和热影响区。在焊合区观察到大量的被细化的铝基体晶粒以及粒径明显减小的 B<sub>4</sub>C 颗粒。在热力影响区出现塑性变形、热影响和被拉长的铝晶粒。

**关键词:** 搅拌摩擦焊; 金属基复合材料; 碳化硼; 接头; 力学性能

(Edited by Hua YANG)